Journal of Applied Mechanics and Technical Physics, Vol. 51, No. 3, pp. 299–307, 2010

MEASUREMENT OF SPECTRAL CHARACTERISTICS OF THE TURBULENT MIXING ZONE

Yu. A. Kucherenko, A. V. Pavlenko, O. E. Shestachenko, S. I. Balabin, A. P. Pylaev, and A. A. Tyaktev

UDC 532.517.4

Experiments with two pairs of gases with different densities with the initial values of the Atwood number A = 0.21 *and* 0.83 *are performed in a multifunctional shock tube. Statistical and spectral characteristics of the mixing zone formed owing to the Richtmyer–Meshkov and Rayleigh–Taylor instability are obtained by the laser sheet technique, and the range of lengths of the main waves in the structure of this zone is determined.*

Key words: *turbulent mixing of gases with different densities, shock tube, Richtmyer–Meshkov and Rayleigh–Taylor instability, laser sheet technique, heterogeneity, concentration spectrum.*

Introduction. A large number of models of turbulent mixing caused by the Richtmyer–Meshkov and Rayleigh–Taylor instability have been developed. In addition to k–ε models, they include models of the second and higher levels of closure [1, 2], whose verification and calibration cannot be performed with the use of integral characteristics of mixing (dimensionless mixing velocity and distributions of the mean density of the substance) obtained in laboratory experiments and require experimentally measured spectral characteristics of time-dependent density and velocity in the mixing zone.

Statistical and spectral characteristics of the turbulent mixing zone formed under the consecutive actions of the Richtmyer–Meshkov and Rayleigh–Taylor instability were obtained for some time instants in the present work by the laser sheet technique [3] in a multifunctional shock tube (MST) at the Institute of Technical Physics [4]. The spectral characteristics are used to estimate the range of lengths of the main waves in the mixing zone.

The structure of the mixing zone of gases with different densities was studied by the laser sheet technique in [5]. The distribution of density of the heavy gas in the laser sheet plane was obtained. A jump in density was found at the boundary between the heavy gas and the mixing zone. This fact contradicted the integral measurements of the density distributions of fluids with different densities, which were performed in [6] by the x-ray technique. Careful calibration of the measurement technique was performed in the present work.

1. Arrangement of Experiments. The experiments were performed in a vertical MST with a square inner cross section 138 × 138 mm; the diagram of the shock tube is shown in Fig. 1. The upper part of the MST contains a section filled with an explosive gas mixture, which is a stoichiometric mixture $H_2 + 0.5O_2$. This section is separated from the ambient atmosphere and from the remaining part of the MST by membranes 1 and 4 made of a Mylar film 20 μm thick. The membranes are located on grids consisting of thin metallic strings 0.1 mm in diameter; the cell size of the grids is 12 × 12 mm. The heavy and light gases are separated from each other by a membrane 6 made of a nitrocellulose film whose thickness is approximately 1 μm. The membrane is located on a grid composed of thin strong strings with a cell size of 6 × 6 mm. The MST sections are filled with gases having a pressure of 10^5 Pa and a temperature of 293 K. In the first series of experiments, the heavy gas was carbon dioxide (CO_2) with a density $\rho_2 = 1.98 \cdot 10^{-3}$ g/cm^3, and the light gas was helium (He) with a density $\rho_1 = 0.178 \cdot 10^{-3}$ g/cm^3; the Atwood number was $A = (\rho_2 - \rho_1)/(\rho_2 + \rho_1) = 0.83$. In the second series of experiments, carbon dioxide and air

Zababakhin Institute of Technical Physics, Snezhinsk 456770; avpavlenko@vniitf.ru. Translated from Prikladnaya Mekhanika i Tekhnicheskaya Fizika, Vol. 51, No. 3, pp. 3–13, May–June, 2010. Original article submitted January 27, 2009; revision submitted May 27, 2009.

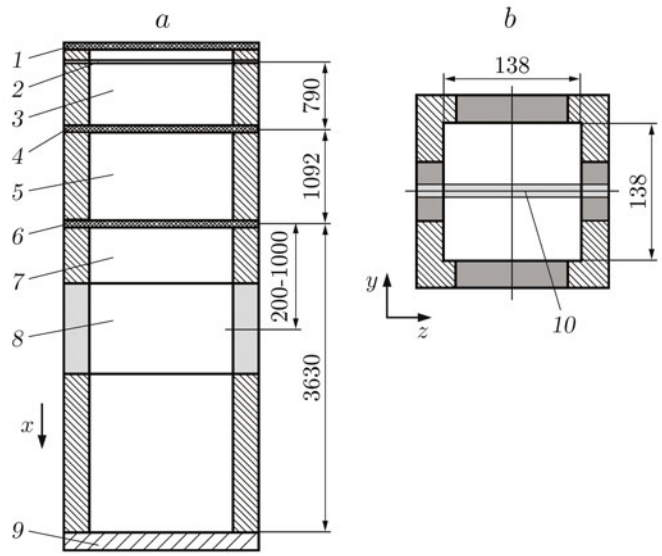

Fig. 1. Schematic diagram of the shock tube: (a) vertical section of the shock tube; (b) cross section of the measurement section; 1, 4) membranes separating the section containing the explosive gas mixture from the ambient air and from the heavy gas, respectively; 2) plane of initiation of the explosive gas mixture; 3) explosive gas mixture; 5) heavy gas; 6) membrane separating the heavy gas from the light gas; 7) light gas; 8) measurement section; 9) shock wave reflector; 10) laser sheet.

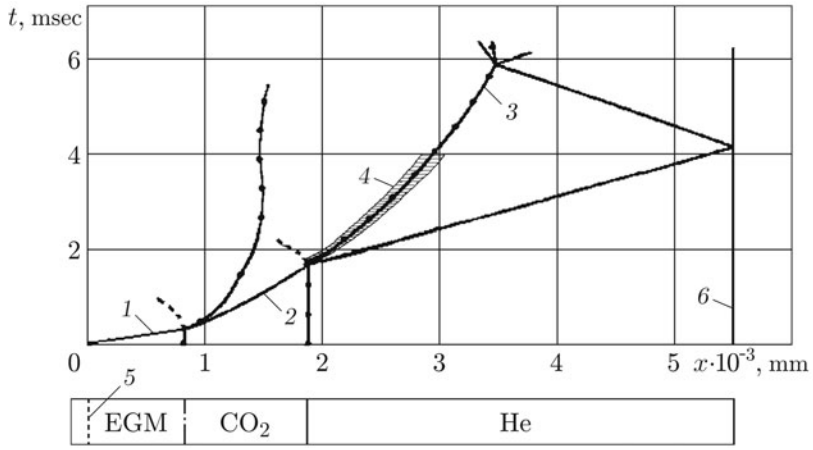

Fig. 2. x–t Diagrams of motion of the shock waves and contact boundaries for the pair of gases CO_2–He: 1) detonation wave; 2) shock wave; 3) initial position of the contact boundary between the gases; 4) zone of turbulent mixing; 5) initiation plane; 6) shock wave reflector; the explosive gas mixture is indicated by EGM.

were used; the Atwood number was A = 0.21. To ensure a sufficient time interval of measurements, the location of the measurement section was changed in the range from 200 to 1000 mm (see Fig. 1).

Twenty three copper conductors 0.1 mm in diameter and 138 mm long were placed parallel to each other with a step of 6 mm in the plane of initiation of the explosive gas mixture. The ohmic resistance of the system of the conductors was $1.3 \cdot 10^{-2}$ Ω; the mass of the conductors was 0.22 g. An electric pulse of energy equal to 1.3 kJ was applied to the conductors during 1.8 μsec. This energy is greater than the energy of copper sublimation (5.2 kJ/g), which leads to an electric explosion of the conductors.

The electric explosion of the conductors induces the detonation of the explosive gas mixture. When the detonation wave reaches membrane 4, a decaying shock wave starts to propagate over the heavy gas. Figure 2 shows the x–t diagrams of motion of the shock waves and contact boundaries for the pair of gases CO_2–He, which

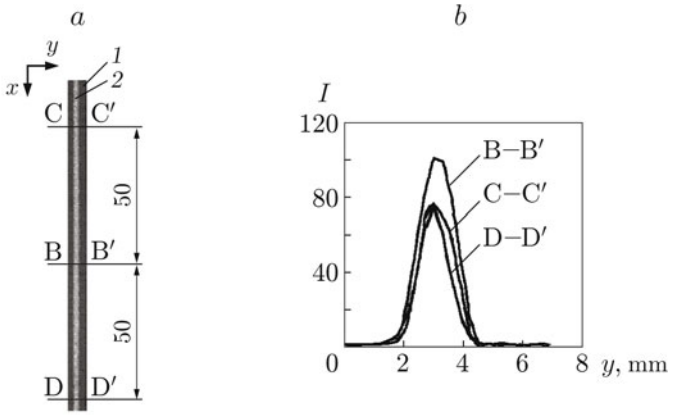

Fig. 3. Measurement of the light intensity in different sections of the plane (x, z) of the laser sheet: (a) section of the laser sheet on the input diaphragm of the MST measurement section; (b) distributions of the light intensity in three sections; 1) input diaphragm of the measurement section; 2) laser sheet section.

were calculated by the Volna program [7]. The position of the mixing zone determined experimentally with the use of the schlieren technique is shown for the same pair of gases. Similar x–t diagrams were calculated for the pair of gases CO_2–air.

The time of arrival of the shock wave on the contact boundary between the heavy and light gases is $t_c = 1.78$ msec. At this instant, the pressure on the wave front is $5.6 \cdot 10^5$ Pa, its velocity is 604 m/sec, and the mass velocity of the gas behind the wave front is 422 m/sec. When the shock wave passes through the contact boundary, there arises the Richtmyer–Meshkov instability, which leads to enhancement of disturbances and to the formation of the turbulent mixing zone. The character of the flow behind the shock wave front is such that the gradients of density and pressure on the contact boundary have the opposite directions. As a result, the Rayleigh–Taylor instability arises, which is responsible for the further evolution of the process.

2. Diagnostics and Calibration. When the mixing zone arrives in the MST measurement section, its photoregistration with the laser sheet technique is performed. The position of the laser sheet in the measurement section is shown in Fig. 1b. The laser sheet was generated by the "Big Sky Laser" pulsed laser with a wavelength of 532 nm and a cylindrical optical system. The characteristics of the laser sheet, which was inhomogeneous both over the cross section and over the area, were measured. The substance used for visualization was the products of thermal decomposition of organic resin (incense). The visualizing particles (V-particles) were uniformly distributed over the entire volume of the gas filling the MST measurement section. Figure 3 shows the section of the laser sheet on the input diaphragm of the MST measurement section and the distributions of the dimensionless intensity of the registered light in three x sections. Figure 4 shows the photograph of the laser sheet obtained in the section $y = \text{const}$ and the distributions of the scattered light intensity in two sections.

As the laser sheet was inhomogeneous, a careful calibration was needed. First of all, the positions of the laser, light flux former, measurement section, and recorder were fixed. The laser power was also constant. These parameters were unchanged both in the calibration of the measurement channel and in experiments. Therefore, the number of light quanta Q incoming from the laser to a certain small elementary volume $\Delta V = \Delta x \times \Delta y \times \Delta z$ of the laser sheet in the vicinity of the point with the coordinates (x, y, z) was identical in each experiment. Because of laser sheet inhomogeneity, the number of quanta Q depends on the location of the volume ΔV. If the laser sheet thickness is sufficiently small, then the number of quanta Q depends only on two coordinates: $Q = Q(x, z)$.

The recorder readings are functions of the number of scattered radiation quanta Q_s incoming from each volume ΔV to the corresponding pixel of the light-sensitive matrix of the recorder: $I = I(Q_s)$. For a constant shape of the optical channel, therefore, the number of scattered quanta Q_s is proportional to the concentration of V-particles n and to the number of light quanta Q incoming from the laser to the volume ΔV: $Q_s \sim nQ(x, z)\Delta V$. Thus, the recorder readings in the case considered depend on the concentration of V-particles and on the coordinates x, z, i.e., $I = I(n, x, z)$. The resultant record is a rectangular matrix consisting of the recorder readings obtained in

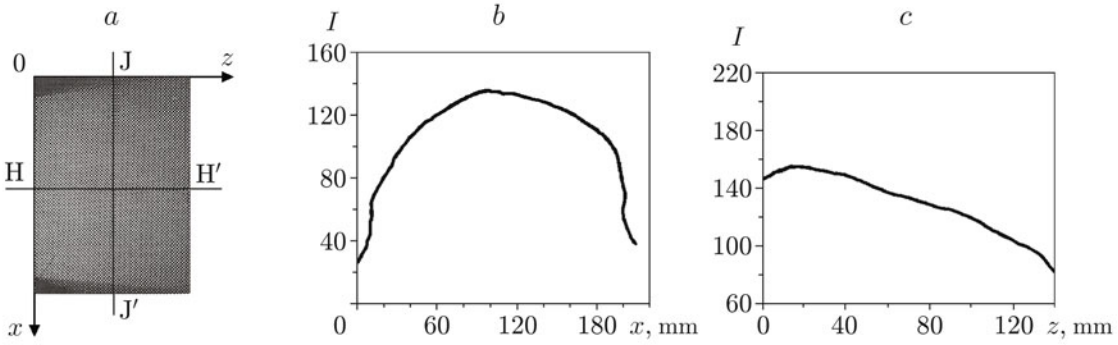

Fig. 4. Measurement of the light intensity in different sections of the planes (x, y) and (y, z) of the laser sheet: photograph of the laser sheet (a) and distributions of the light intensity in J–J′ section (b) and H–H′ section (c).

each pixel of the light-sensitive matrix:

$$I = I(n, x, z) \equiv \{I(n, x_i, z_j)\} \equiv \{I_{i,j}(n)\}, \qquad i = 1, 2, \ldots, m, \quad j = 1, 2, \ldots, k.$$

Here, m and k are the numbers of pixels of the light-sensitive matrix of the recorder in the x and z directions, respectively, x_i and z_j are the coordinates of points in the registration region, which are projected by the optical system to the corresponding pixel.

During the calibration, the MST measurement section was filled with the heavy gas having a pressure of 10^5 Pa; V-particles (products of thermal decomposition of incense) were added to this gas. The calibration was performed for seven values of the concentration to include all possible values of the concentration of V-particles in experiments. Ten measurements were performed for each value of the concentration of V-particles. As a result, we obtained seven calibration matrices with each cell containing the intensity of light scattered by V-particles from the corresponding area of the laser sheet, which was averaged over ten measurements. In experiments on measurement of spectral characteristics of the mixing zone, the result of registration was also a matrix with each cell containing the intensity of light scattered by V-particles; the size of this matrix coincided with the size of the calibration matrices. The concentration of V-particles corresponding to a given cell of the experimental matrix was determined by linear interpolation between two neighboring values of the light intensity in the corresponding cells of the calibration matrices. As a result, each experiment provided a matrix of concentrations of V-particles $\{n_{ij}\}$. As the mixing zone boundaries had different coordinates along the x and z axes in different experiments, the coordinates of the points x_i and z_j were numerated anew. In the new coordinates, the value $i = 1$ corresponded to the boundary between the mixing zone and the heavy has, and the value $i = m_1$ corresponded to the boundary between the mixing zone and the light gas, respectively. The values $j = 1$ and $j = k_1$ for the points along the z axis were determined by the width of the zone of near-wall flows.

The matrices of concentrations $\{n_{ij}\}$ were normalized to the concentration n_0 of V-particles, which were in the heavy gas outside the mixing zone at the moment of registration. As a result, we obtained a matrix of normalized concentrations $\{N_{ij}\}$, where $N_{ij} = n_{ij}/n_0$. We can assume that V-particles are "frozen" into the gas, i.e., do not leave the gas particle where they were initially in the course of the experiment. Then, the concentration of V-particles is directly related to the heavy gas concentration. Therefore, the matrix $\{N_{ij}\}$ contains the values of the normalized concentration of the heavy gas.

For convenience of further processing of experimental results, we introduced a dimensionless coordinate $\xi = (x - x_1)/(x_{m1} - x_1)$; the value $\xi = 0$ corresponds to the boundary between the mixing zone and the heavy gas, and the value $\xi = 1$ is the boundary between the mixing zone and the light gas. In addition, we have $N_{1j} = 1$ and $N_{m1j} = 0$. The relative error of determining the concentration in one experiments with allowance for all factors (incense mass, distribution of incense particles over the gas volume, scatter of the laser radiation intensity, inhomogeneity of the laser sheet, and interpolation error) was smaller than 5%.

3. Determination of Statistical and Spectral Characteristics of the Mixing Zone. The characteristics of the mixing zone were measured for each pair of gases in three series of experiments corresponding to three instants of registration. Each series included 15 experiments, which provided a set of normalized concentrations

of the heavy gas, which was sufficient for statistical processing. The processing was performed for the coordinate values $\xi = 0.1$, 0.3, 0.5, 0.7, and 0.9. Each of these values corresponds to its own row in the matrix of normalized concentrations of the heavy gas (in the z direction) obtained from the experiment. The rows corresponding to the considered values of ξ were united. As a result, for each of the three registration instants, we obtained five statistical distributions of the normalized concentration of the heavy gas $\{N_j(\xi)\}$ $(j = 1, 2, \ldots, K)$ with an identical z interval of discreteness for all distributions, which was equal to $\Delta z = 0.14$ mm. The values of K for different experiments were different and lied within the range $10{,}920 \leqslant K \leqslant 12{,}780$. This is explained by the fact that the processing domain did not include the zone of near-walls flows, which had different sizes in different experiments.

Further processing was performed in the following way. First of all, for each value of ξ, the distribution of the concentration $N_j(\xi)$ was expanded into a finite Fourier series as

$$N_j(\xi) = A_0 + \sum_{k=1}^{K/2} A_k \cos\frac{2\pi jk}{K} + \sum_{k=1}^{K/2-1} B_k \sin\frac{2\pi jk}{K}, \qquad j = 1, 2, \ldots, K, \tag{1}$$

where A_0, A_k, and B_k are the coefficients:

$$A_0 = \frac{1}{K}\sum_{j=1}^{K} N_j, \quad A_k = \frac{2}{K}\sum_{j=1}^{K} N_j \cos\frac{2\pi jk}{K}, \quad B_k = \frac{2}{K}\sum_{j=1}^{K} N_j \sin\frac{2\pi jk}{K}, \quad k = 1, 2, \ldots, \frac{K}{2}.$$

As the Kotel'nikov theorem reads that the spatial cutoff frequency is $f_c = 1/(2\Delta z)$, then the number of harmonics in the expansion in Eq. (1) is half the number of the concentration values. After that, terms containing wavelengths $\lambda \geqslant \lambda_0$, where $\lambda_0 = 100$ mm, were eliminated. This range of wavelengths was determined neither by the initial nor the boundary conditions of experiments, but occurred only owing to formation of the total zone of processing in the z direction by uniting the distributions obtained in experiments for this time instant. The number of the harmonic k_0 corresponding to the wavelength λ_0 is determined by the relation

$$k_0 = K\Delta z/\lambda_0.$$

Then, the expression for the normalized concentration of the heavy gas can be written as

$$N_{\lambda j}(\xi) = A_0 + \sum_{k=k_0}^{K/2} A_k \cos\frac{2\pi jk}{K} + \sum_{k=k_0}^{K/2-1} B_k \sin\frac{2\pi jk}{K}, \qquad j = 1, 2, \ldots, K.$$

The mean value of the normalized concentration of the heavy gas was determined by the formula

$$\langle N_\lambda(\xi)\rangle = \frac{1}{K}\sum_{j=1}^{K} N_{\lambda j}(\xi).$$

The formula for the heterogeneity coefficient $\Gamma = 1 - \theta$ has the form

$$\Gamma(\xi) = \frac{\langle N'_\lambda(\xi) N'_\lambda(\xi)\rangle}{\langle N_\lambda(\xi)\rangle(1 - \langle N_\lambda(\xi)\rangle)}, \tag{2}$$

where $\langle N'_\lambda(\xi)N'_\lambda(\xi)\rangle = \dfrac{1}{K}\displaystyle\sum_{j=1}^{K} N'_{\lambda j}(\xi)N'_{\lambda j}(\xi)$ is the mean value of the squared fluctuations, $N'_{\lambda j}(\xi) = N_{\lambda j}(\xi) - \langle N_\lambda(\xi)\rangle$ are the concentration fluctuations, and $\theta(\xi)$ is the coefficient of homogeneity of the mixture of two incompressible substances [8]:

$$\theta(\xi) = \frac{\langle N_\lambda(\xi)[1 - N_\lambda(\xi)]\rangle}{\langle N_\lambda(\xi)\rangle\langle 1 - N_\lambda(\xi)\rangle}.$$

The estimate of compressibility of the gases for the gas-dynamic flow parameters obtained in the experiments performed gives a correction smaller than 5%; therefore, the influence of compressibility was ignored.

The autocorrelation function was determined by the formula [9]

$$R(\xi, r) = \frac{1}{K - r}\sum_{j=0}^{K-r} N'_{\lambda,j}(\xi)N'_{\lambda,j+r}(\xi), \qquad r = 0, 1, 2, \ldots, r_0, \quad r_0 = \lambda_0/\Delta z,$$

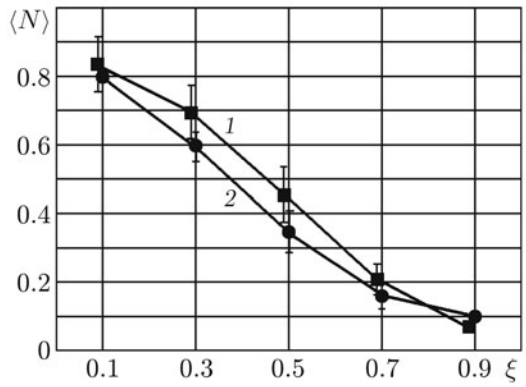

Fig. 5. Mean values of the normalized concentration of the heavy gas versus the coordinate ξ: curve 1 refers to the pair of gases CO_2–air and curve 2 refers to the pair of gases CO_2–He.

and the spectral density of the mean square of fluctuations of the normalized concentration of the heavy gas was found by the formula [9]

$$G(\xi, f) = 2\Delta z\Big(R_0(\xi) + R_{r_0}(\xi)\cos\frac{\pi r_0 f}{f_c} + 2\sum_{r=1}^{r_0-1} R_r(\xi)\cos\frac{\pi r f}{f_c}\Big), \tag{3}$$

where $f = 1/\lambda$ is the spatial frequency.

The autocorrelation function was used to calculate the spectral density and to process the experimental distributions obtained. As the area under the spectral density curve in the entire range of frequencies is equal to the mean square of fluctuations, function (3) makes it possible to estimate the range of the main waves in the mixing zone.

4. Results of Experiments. In the experiments, we measured the mixing zone at three time instants t_r. In the first series of experiments (gases CO_2–He), we had $t_r = 2.1$, 2.6, and 3.1 msec; in the second series of experiments (gases CO_2–air), we used $t_r = 3.2$, 4.0, and 6.4 msec. Figure 5 shows the mean values of the normalized concentration of the heavy gas in the mixing zone as functions of the coordinate ξ and the standard deviations obtained in these experiments. For each value of ξ, the averaging was performed both over the coordinate z and over the three instants of registration. The heavy gas concentration is seen to decrease monotonically with increasing the coordinate ξ. As a whole, the dependences agree well with the distributions of the mean density of the substance in the mixing zone, which were obtained in [6] by x-ray measurements. For the Atwood number A = 0.21, the mean value of the heavy gas concentration in the middle of the turbulent mixing zone ($\xi = 0.5$) is $\langle N\rangle = 0.453 \pm 0.090$; for A = 0.83, we have $\langle N\rangle = 0.351 \pm 0.060$. The difference of these values from $\langle N\rangle = 0.5$ is caused by the asymmetry arising in the Rayleigh–Taylor turbulent mixing; at A = 0.83, the asymmetry is more pronounced than at A = 0.21. This result is consistent with the known results [6, 10]. Note that the dependences in Fig. 5 are substantially different from the distribution of the relative density of the heavy gas, which was obtained in [5]. According to [5], the relative density of the heavy gas in the middle of the turbulent mixing zone for the pair of air and He is 0.2, which also contradicts the results of [9, 10].

Figure 6 shows the heterogeneity coefficient calculated by Eq. (2) and averaged over ξ as a function of the time of mixing zone evolution from the moment when the shock wave reaches the contact boundary between the gases $t' = t_r - t_c$. It is seen that the heterogeneity coefficient averaged over the mixing zone for both pairs of gases considered reaches the limiting value rather rapidly; this limiting value is $\langle\Gamma\rangle_{\rm lim} = 0.13$ for A = 0.21 and $\langle\Gamma\rangle_{\rm lim} = 0.18$ for A = 0.83. The limiting values $\langle\Gamma\rangle_{\rm lim}$ correspond to the range of the heterogeneity coefficient 0.15–0.25 obtained in model calculations [8, 11–13].

Figure 7 shows the spectral density of the mean square of fluctuations of the normalized concentration of the heavy gas as a function of the spatial frequency $G(f)$ for two pairs of gases at different time instants. The maximum relative root-mean-square error of determining the mean square of concentration fluctuations is smaller than 6%. The time is counted from the moment of shock wave arrival on the contact boundary between the gases. It is seen that there is a range of frequencies where the values of the spectral density differ substantially from zero. A comparison of the dependences $G(f)$ obtained for different time instants shows that these ranges of

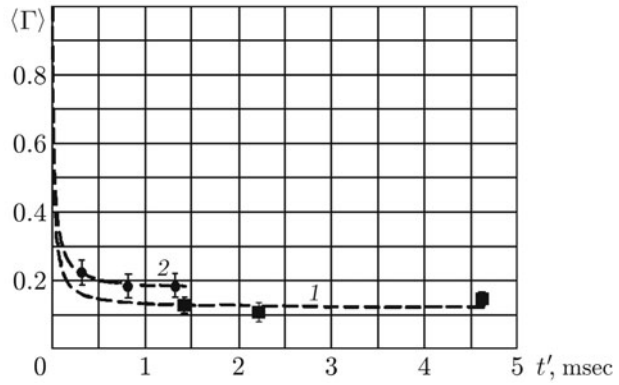

Fig. 6. Heterogeneity coefficient in the mixing zone versus the time t': curve 1 refers to the pair of gases CO_2–air and curve 2 refers to the pair of gases CO_2–He.

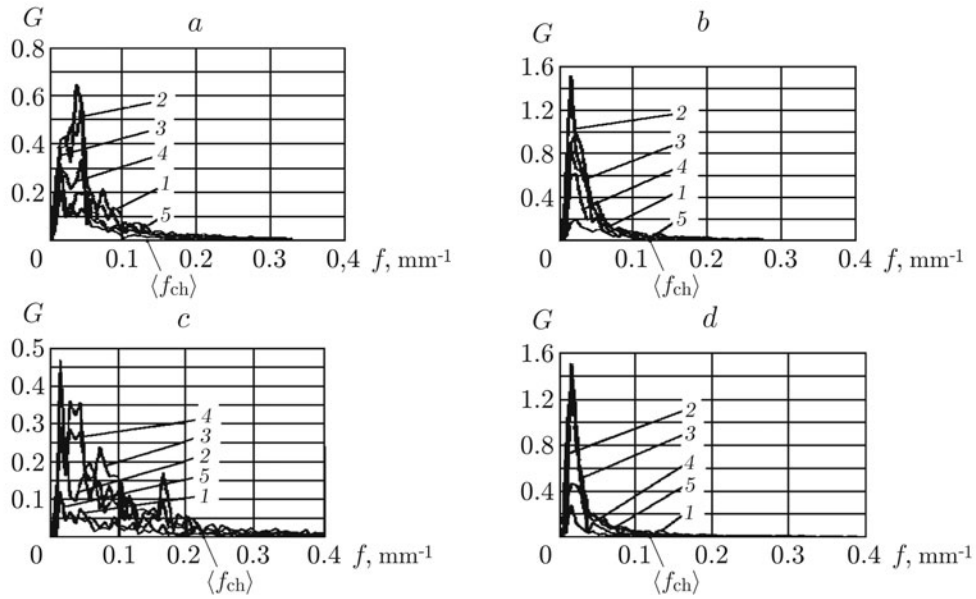

Fig. 7. Spectral density versus the spatial frequency in the mixing zone for $\xi = 0.1$ (1) 0.3 (2), 0.5 (3), 0.7 (4), and 0.9 (5): (a, b) pair of gases CO_2–He at $t' = 0.32$ (a) and 1.32 msec (b); (c, d) pair of gases CO_2–air at $t' = 1.42$ (c) and 4.62 msec (d).

frequencies become narrower with time and are shifted toward lower frequencies. We can try to characterize the range of frequencies (lengths) of the main waves in the mixing zone with the use of the characteristic frequency $f_{\text{ch}}(\xi)$ [characteristic wavelength $\lambda_{\text{ch}}(\xi) = 1/f_{\text{ch}}$] determined by the relation

$$f_{\text{ch}}(\xi) = \int_0^{f_c} fG(f,\xi)\,df \;\Big/\; \int_0^{f_c} G(f,\xi)\,df$$

($f_c = 3.6$ mm^{-1} is the cutoff frequency). It follows from Fig. 7 that the values of $\langle f_{\text{ch}}\rangle$ averaged over ξ are actually the boundaries of the ranges from the side of higher frequencies. The corresponding values of the characteristic wavelengths $\langle\lambda_{\text{ch}}\rangle$ averaged over ξ are the boundaries of the ranges from the side of shorter waves. The dependences of these values (determined with a relative root-mean-square error smaller than 10%) on the time of mixing zone development are plotted in Fig. 8. It is seen that the values of $\langle\lambda_{\text{ch}}\rangle$ for the gas pairs considered increase with time, and this increase for the pair of gases CO_2–He (A = 0.83) is more pronounced than for the pair of gases CO_2–air (A = 0.21). This result agrees with the general laws of the Rayleigh–Taylor turbulent mixing.

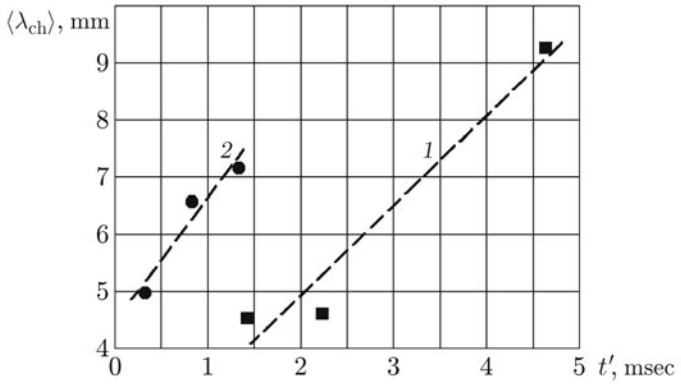

Fig. 8. Characteristic wavelengths versus the time of development of the mixing zone: curve 1 refers to the pair of gases CO_2–air and curve 2 refers to the pair of gases CO_2–He.

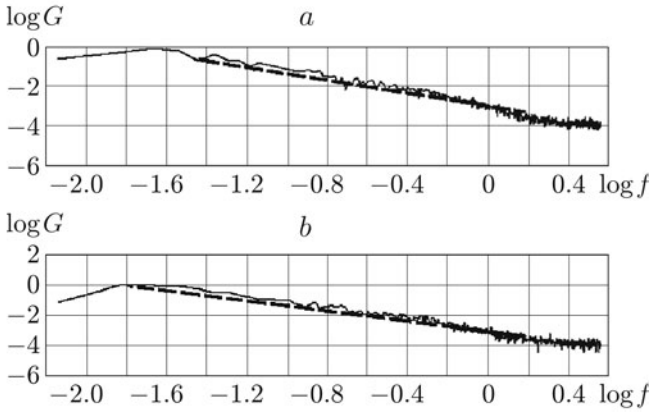

Fig. 9. Spectral density versus the spatial frequency: (a) pair of gases CO_2–air ($t' = 2.22$ msec); (b) pair of gases CO_2–He ($t' = 1.32$ msec); the dashed curves show the dependence $\log G \approx -(3 + (5/3) \log f)$.

In the case of isotropic turbulence, there is an interval of the spectral function of the mean square of fluctuations of scalar quantities, where the dependence of this function on frequency has a power-law character with a power index equal to $-5/3$ [14]. In this interval, the turbulent energy in transferred from large-scale structures of the mixing zone to small-scale structures with subsequent dissipation of the turbulent energy. It is of interest to know whether the spectral functions of the mean square of fluctuations of the normalized concentration possess such a property. For this purpose, for each value of ξ, we plotted the spectral density as a function of frequency in the logarithmic scale $\log G = F(\log f)$. Figure 9 shows such dependences at $\xi = 0.5$ for two pairs of gases. It is seen that the spectral functions in the case considered also possess this property: there is an interval where the dependence $G(f)$ can be presented in the form $G \sim f^{-5/3}$.

Conclusions. Distributions of the normalized concentration of gases over the turbulent mixing zone formed after passage of an unsteady shock wave through the contact boundary were obtained for two pairs of gases with different densities (CO_2–air and CO_2–He). The values of the heterogeneity coefficient of the mixture and the spectral density of the mean square of fluctuations of the normalized concentration of the heavy gas were obtained for the first time by the laser sheet technique. The ranges of lengths of the main waves in the mixing zone were determined. It was demonstrated that there is an interval for the spectral function of the mean square of concentration fluctuations, where the dependence of this function on frequency has a power-law character with a power index of $-5/3$. A careful calibration of the measurement technique of the heavy gas concentration provided a concentration distribution that differs from the distribution obtained in [5], but agrees with the results of [9, 10].

This work was supported by the International Science and Technology center (Grant No. 2716).

REFERENCES

1. O. Gregoire and D. Soufland, "Simulations of compressible mixing flows using a second order turbulent model," in: *Proc. of the 7th Int. Workshop on the Physics of Compressible Turbulent Mixing* (St.-Petersburg, Russia, July 5–9, 1999), Inst. of Exp. Phys., Sarov (2001), pp. 252–258.
2. Z. Zhang and J. Wang, "Numerical simulations of Rayleigh–Taylor instability with the simplified Reynolds stress model," in: *Proc. of the 6th Int. Workshop on the Physics of Compressible Turbulent Mixing* (Marseilles, France, June 18–21, 1997), Univ. of Provence, Marseilles (1997), pp. 569–574.
3. D. Landeg, M. Philpott, I. Smith, and A. Smith, "The laser sheet as a quantitative diagnostic in shock tube experiments," in: *Proc. of the 4th Int. Workshop on the Physics of Compressible Turbulent Mixing* (Cambridge, England, March 29–April 1, 1993), Cambridge Univ. Press, Cambridge (1993), pp. 230–239.
4. Yu. A. Kucherenko, O. E. Shestachenko, S. I. Balabin, and A. P. Pylaev, "RFNC-VNIITF multifunctional shock tube for investigating the evolution of instabilities in non-stationary gas dynamic flows," *Laser Particle Beams*, **21**, 381–384 (2003).
5. E. E. Meshkov, V. V. Nikiforov, and A. I. Tolshmyakov, "Structure of the turbulent mixing zone on the boundary of two gases accelerated by a shock wave," *Combust., Expl., Shock Waves*, **26**, No. 3, 315–320 (1990).
6. Yu. A. Kucherenko, L. I. Shibarshov, V. I. Chitajkin, et al., "Experimental study of the gravitational turbulent mixing self-similar mode," in: *Proc. of the 3rd Int. Workshop on the Physics of Compressible Turbulent Mixing* (Royaumont, France, June 17–19, 1991), S. n., Royaumont (1991), pp. 427–454.
7. V. F. Kuropatenko, G. V. Kovalenko, V. I. Kuznetsov, et al., "The VOLNA software and inhomogeneous difference method for calculating unsteady motion of compressible continua," in: *Problems of Atomic Science and Engineering. Mathematical Modeling of Physical Processes* (collected scientific papers) [in Russian], No. 2 (1989), pp. 9–25.
8. D. L. Youngs, "Direct three-dimensional numerical simulation of mixing by Rayleigh–Taylor instability," in: *Proc. of the 4th Int. Workshop on the Physics of Compressible Turbulent Mixing* (Cambridge, England, March 29–April 1, 1993), Cambridge Univ. Press, Cambridge (1993), pp. 167–177.
9. J. S. Bendat and A. G. Piersol, *Random Data: Analysis and Measurement Procedures*, Wiley-Interscience, New York (1971).
10. K. Read, "Experimental investigation of turbulent mixing by Rayleigh–Taylor instability," *Physica D*, **12**, 45–58 (1984).
11. A. S. Kozlovskih and D. V. Neuvazhayev, "Coefficient of heterogeneity in turbulent mixing zone," *Laser Particle Beams*, **18**, 207–212 (2000).
12. D. L. Youngs, "Three-dimensional simulation of turbulent mixing by Rayleigh–Taylor instability," *Phys. Fluids*, **A3**, 1312–1320 (1991).
13. V. E. Neuvazhayev, A. F. Podkoritova, V. G. Jakovlev, et al., "Comparing the models of turbulent mixing induced by the Rayleigh–Taylor and the Richtmyer–Meshkov instabilities," in: *Proc. of the 3rd Int. Workshop on the Physics of Compressible Turbulent Mixing* (Royaumont, France, June 17–19, 1991), S. n., Royaumont (1991), pp. 477–482.
14. S. Corrsin, "On the spectrum of isotropic temperature fluctuations in an isotropic turbulence," *J. Appl. Phys.*, **22**, No. 4, 469–473 (1951).